RSC Advances

PAPER

View Article Online
View Journal | View Issue

Cite this: *RSC Adv.*, 2015, **5**, 76825

Selective enhancement of red emission from upconversion nanoparticles *via* surface plasmon-coupled emission†

Ai Ling Feng,[abc] Min Lin,*[acd] Limei Tian,[e] Hong Yuan Zhu,[ac] Hui Guo,[ac] Srikanth Singamaneni,[e] Zhenfeng Duan,[d] Tian Jian Lu[c] and Feng Xu*[ac]

Upconversion nanoparticles (UCNPs) can convert low-energy light (*e.g.* near-infrared, NIR) to high-energy light (*e.g.* visible). UCNPs such as $NaYF_4$:Yb,Er will generate strong green emission at 540 nm and weak red emission at 650 nm. Considering the "optical window" of cells and tissues (600–900 nm) owing to the lack of efficient endogenous absorbers, red emission (600–700 nm) enhancement is especially important for deep tissue imaging. Therefore, it is of great significance to selectively enhance red emission of UCNPs. Placing UCNPs in proximity to gold nanorods (AuNRs) can enhance the emission of UCNPs. In this paper, we fabricate heteronanostructures composed of UCNPs and AuNRs and precisely control the distance with polyelectrolyte multilayers as spacers to enhance the red emission of UCNPs. Fluorescence spectra of UCNPs enhanced by AuNRs with different thicknesses of polyelectrolyte are measured. The results show that red emission intensity exhibits a strong dependence on the interparticle distance and spectral properties of these nanoparticles. At a optimized distance of 8 nm, the maximal fluorescence enhancement of 10.6-fold for red emission is achieved by tuning the localized surface plasmon resonance (LSPR) wavelength of AuNRs to match with the red emission. The enhancement of the red emission is further confirmed by a decreased decay time induced by surface plasmon-coupled emission (SPCE). The enhancement also contributes to the increased penetration depth from 7.5 mm to 12.5 mm. These results reveal that our strategy possesses the ability of selectively enhancing red emission of UCNPs and provides theoretical guidance on preparing versatile systems with enhanced red emission by the SPCE effect.

Received 6th July 2015
Accepted 24th August 2015

DOI: 10.1039/c5ra13184g

www.rsc.org/advances

Introduction

NIR light and red emission are referred to as the 'optical window' of cells and tissues owing to the lack of efficient endogenous absorbers in this range and the subsequently high penetration depth.[1] Therefore, red emission has attracted special attention for bioimaging applications. Among the various bioimaging labels, lanthanide-doped UCNPs have emerged as highly promising nanoprobes, as they can emit visible light when excited by NIR light.[2,3] Additionally, UCNPs demonstrate attractive advantages including long fluorescence lifetime and minimized autofluorescence, which overcome the limitations associated with fluorophores and quantum dots.[3–6] However, UCNPs suffer from low quantum yields due to their small absorption cross sections attributed to formally forbidden f-level atom transitions of the lanthanide ions.[7] Besides, a variety of quenchers on the UCNPs surface as induced by surface defects can lead to quenching effect and reduced quantum yield.[8] All these will reduce fluorescence emission including red emission from UCNPs. Therefore, there is an urgent need to selectively enhance red emission from UCNPs to achieve deeper tissue penetration capacity.

Various strategies have been employed to enhance fluorescence emission of UCNPs. One approach is by material design, such as tailoring doping ion concentration, optimizing host composition and phase, and avoiding quenching from surface defects by preparing a core–shell nanostructure.[5,9–18] Among these, preparing a homogeneous core–shell nanostructure is a very common method to enhance fluorescence. The shell of a homogeneous core–shell nanostructure (such as $NaYF_4$:Yb,Er@$NaYF_4$) can generate a strong suppression of surface

[a]*The MOE Key Laboratory of Biomedical Information Engineering, School of Life Science and Technology, Xi'an Jiaotong University, Xi'an 710049, P.R. China. E-mail: fengxu@mail.xjtu.edu.cn; minlin@mail.xjtu.edu.cn*

[b]*Institute of Physics & Optoelectronics Technology, Baoji University of Arts and Sciences, Baoji 721016, China*

[c]*Bioinspired Engineering and Biomechanics Center (BEBC), Xi'an Jiaotong University, Xi'an 710049, P.R. China*

[d]*Center for Sarcoma and Connective Tissue Oncology, Massachusetts General Hospital, Harvard Medical School, MA 02114, USA*

[e]*Department of Mechanical Engineering and Materials Science, Institute of Materials Science and Engineering, Washington University in St. Louis, St Louis, MO 63130, USA*

† Electronic supplementary information (ESI) available. See DOI: 10.1039/c5ra13184g

deactivations and spatial isolation between the core and the deactivators.[19] The dopant ions are therefore limited in the interior $NaYF_4$:Yb,Er core, suppressing energy transfer and resulting in enhanced fluorescence.[5] For example, $NaYF_4$:Yb,Er@$NaYF_4$ has been studied and enhanced fluorescence of about 7-fold have been achieved by coating a ~2 nm thick $NaYF_4$ shell on the $NaYF_4$:Yb,Er core.[20] However, the ultrathin coating thickness is difficult to precisely modulation. Meanwhile, Mai *et al.*[21] found <1 fold enhanced fluorescence for $NaYF_4$:Yb,Er@$NaYF_4$ core–shell nanostructure. Therefore, the extent of enhanced fluorescence varies in different reports. Another route is plasmon enhancement by placing UCNPs in proximity to metal nanoparticles (*i.e.* Au).[22–25] Several studies reported plasmon enhancement of UCNPs by different technologies including placing UCNPs surrounding metal surfaces[25,26] and employing core–shell nanostructures with either plasmon cores[27,28] or shells.[24,29,30] The plasmon enhancement mechanism is mainly attributed to local field enhancement (LFE) effect and surface plasmon-coupled emission (SPCE) effect.[14] LFE effect plays a key role when the plasmon frequency of metal nanoparticles matches with the excitation frequency of UCNPs, while SPCE effect can lead to fluorescence efficiency enhancement when LSPR frequency of metal nanoparticles overlaps with the emission of UCNPs.[31–33] Therefore, the plasmon enhancement caused by two effects has a strong dependence on spectral properties of these nanoparticles. On the other hand, non-radiative energy transfer (NRET) effect from fluorescence materials to metal nanoparticles will quench the fluorescence emission.[28,34] The equilibrium of LFE, SPCE and NRET effects has a intimate relationship with the distance between UCNPs and metal nanoparticles. Therefore, the influence of distance and spectral properties on fluorescence enhancement need to be explored.

Several works have contributed to the enhancement of green and red emission of UCNPs by plasmon enhancement. For instance, Li *et al.*[35] investigated $NaYF_4$:Yb,Er@SiO_2@Au core–shell nanostructures for enhanced green emission by tuning the LSPR frequency of Au nanoparticles matching with green emission of UCNPs. Very recently, we have enhanced 22.6-fold fluorescence in green region caused by LFE effect with a novel distance-controlled strategy.[33] However, green emission is limited in bioimaging application. Until now, few studies focusing on upconversion red emission from UCNPs have been reported. Kim *et al.*[29] revealed that red emission was enhanced by tuning the LSPR wavelength of AuNRs through varying the aspect ratio of AuNRs to overlap with red emission of $NaYF_4$:Yb,Er. However, it is lack of precisely modulation of the spacer thickness in a wide range. Therefore, it is still necessary to design high-performance nanostructure with well-controlled spacer thickness in a wider range to achieve bright red emission.

In this study, we reported a novel strategy to fabricate UCNPs and AuNRs heteronanostructures and precisely controlled the spacer thickness by polyelectrolyte multilayers at nanoscale using layer-by-layer assembly process. We have concluded that the emission enhancement of red emission from UCNPs decorated by AuNRs depends on both the distance and the spectra properties of AuNRs. We enhanced the red emission *via* SPCE effect and achieved deeper tissue penetration capacity. These findings reveal that our strategy possesses the ability of selectively enhancing red emission of UCNPs and provides a theoretical guidance of preparing versatile systems with enhanced red emission by SPCE effect for their bioapplications.

Experimental

Synthesis of $NaYF_4$:Yb,Er@PAA upconversion nanoparticles

By thermal decomposition method,[36] oil-soluble $NaYF_4$:Yb,Er upconversion nanoparticles can be synthesized. Rare-earth element chlorides including $YCl_3 \cdot 6H_2O$ (0.80 mM), $YbCl_3 \cdot 6H_2O$ (0.18 mM) and $ErCl_3 \cdot 6H_2O$ (0.02 mM) were added into 2 mL nanopure water with strong sonication to ensure forming a transparent solution. The solution was further put into a mixture of octadecene (15 mL) and oleic acid (6 mL) in a flask, and then stirred at a low rate for 30 min. The solution was further heated to 150 °C in an electromantle with the Argon gas protection at a rate of 10 °C min^{-1} and cooled to room atmosphere gradually. A pre-dissolved mixture of NaOH (2.5 mM) and NH_4F (4 mM) in 5 mL methanol was dripped into the three-necked flask and magnetic stirred for 2 hours at ambient temperature. The mixture was slowly heated to 100 °C and maintained at this temperature for 30 min to remove methanol. It was raised to 280 °C at a rate of 20 °C min^{-1} and then kept at this temperature for 90 min under the protection of Ar gas. The mixture was precipitated by adding an excess amount of ethanol after it cooled down naturally. It was then washed for three times with a mixed solvent of ethanol and cyclohexane (1 : 1).

Poly(acrylic acid) (PAA, $M_w \sim 1800$) is used to replace the original hydrophobic ligands on the surface of $NaYF_4$:Yb,Er with a simple ligand-exchange method. About 1 mL of chloroform solution of UCNPs with the concentration of 15 mg ml^{-1}, 14.5 μL PAA and 1 mL ethanol were mixed together and stirred with 24 h. The mixture was centrifuged at 8000 rpm for 5 min. After washing three times, the as-synthesized nanocrystals were re-dispersed in water. Then the final product $NaYF_4$:Yb,Er@PAA was stored at 4 °C refrigerator.

Preparation of CTAB-coated AuNRs

AuNRs were prepared by a seed-mediated method.[37,38] The seed solution was obtained by adding an ice-cold sodium borohydride solution (10 mM, 0.6 mL) into the mixture (10 mL) of cetyltrimethylammonium bromide (0.1 M) and chloroauric acid (2.5×10^{-4} M) under vigorous stirring condition. Growth solution was obtained by mixing 0.1 M CTAB (100 mL), $HAuCl_4$ (10 mM, 5 mL), silver nitrate (10 mM, 1.0 mL) and ascorbic acid (0.1 M, 0.55 mL) consecutively. Then 0.12 mL seed solution was added and kept in the darkroom. LSPR wavelength of AuNRs can be tailored to 670, 725, 810 nm by varying the amount of $HAuCl_4$ as 4.5, 4.75 and 5.0 mL in the above standard procedure, respectively. The product was centrifuged at 10 000 rpm for 5 min. After washing twice, the as-synthesized nanoparticles were re-dispersed in water.

Fabrication of polyelectrolyte separated UCNPs and AuNRs heteronanostructures

Polyelectrolyte separated UCNPs and AuNRs heteronanostructures were obtained as the following procedures. Silicon substrates were cut into rectangles with the size of 20 × 20 mm^2 and immersed in a piranha solution to be washed three times with nanopure water. Positive-charged AuNRs was electrostatically adsorbed on the surface of negative-charged silicon substrates. Positive-charged PAH (1 mM) and negative-charged PSS (1 mM) polymer were each added in 0.1 M NaCl solution by stirring to form a transparent solution, respectively. Polyelectrolyte layers as spacers were coated alternatively by immersing silicon substrates into the above-mentioned solution for 15 min. By coating polyelectrolyte terminated by a PAH polyelectrolyte, we uniformly precipitated the negative-charged UCNPs–PAA onto silicon substrates. After each precipitation step, the samples were washed with nanopure water for three times and blown with nitrogen gas flow.

Deep-tissue fluorescence imaging

The imaging setup was equipped according our previous reported ones.[33] The power density of the laser is 25 mW mm^{-2} with the excitation of 980 nm. We performed the imaging analysis with different thickness of nylon phantom covering the tested samples to study the penetration capacity. Four kinds of phantoms with the thickness of 5.0, 7.5, 10.0 and 12.5 mm were machined into rectangular with the size of 20 × 20 mm^2. The incident from laser has an angle of 45 degrees with the nylon phantom. A Nikon D90 digital camera was used as a receptor to collect red light emitted from the samples coved by the phantoms. Both the green light emitting from UCNPs and the NIR light scattering from the samples were all filtered away by placing a filter in the front of the camera. The photographs were taken in a darkroom for 30 s and then post-treated in pseudo-color form.

Structural characterization and fluorescent analysis

Representative TEM images of UCNPs and AuNRs were obtained by a JEOL JEM 2100 microscope. SEM images were achieved by a JSM-6700F microscope. A Nano-ZS90 potential analyzer was manipulated to analyze zeta potentials of different nanoparticles. Atomic force microscopy (AFM) characterization was performed in light tapping mode on a DI Innova AFM (Bruker). The absorption spectra of nanoparticles were measured by a UV-3600 UV-Vis-NIR absorption spectrophotometer. Upconversion fluorescence was recorded by QuantaMasterTM40 spectrofluorometer excited by a 980 nm laser. Fluorescence lifetime were tested on an FLsp920 spectrofluorometer (Edinburgh), which is a time-gated method compatible with the long lifetime of UCNPs. Optical photos were taken by a Nikon D90 digital camera under the excitation of 980 nm laser for 30 s in the tissue penetration depth experiment.

Simulations

The electric field around the AuNRs was simulated on the commercial finite-element-method based solver (Comsol Multiphysics software 4.4) under 980 nm excitation. All the structures were meshed by tetrahedral mesh element varied from 0.1 nm to 40 nm. The boundary of the simulation was a perfectly matched layer. The permittivity for gold nanoparticles was set using an analytic model provided by Etchegoin *et al.*[39] The light source was considered as a plane wave at 980 nm excitation with an incidence direction perpendicular to the long axis. In the model the AuNRs was equivalent to a nanosphere with the same aspect ratio and axial length. And the UCNPs were considered as a dipole placed on the long axis of the spheroid with averaged polarization in space. The quantum efficiency enhancement was achieved by improved Gersten and Nitzan model.[40] And the refractive index was set as 1 which was equal to that in air.

Results and discussion

Experimental strategy of designing polyelectrolyte separated UCNPs and AuNRs heteronanostructures

To study ultra-bright fluorescence nanomaterials for deep-tissue bioimaging, novel polyelectrolyte separated UCNPs and AuNRs heteronanostructures were designed and fabricated without need for any complicated procedures, Scheme 1a. The heteronanostructures were constructed using polyelectrolyte multilayers as spacers to precisely tune the distance between UCNPs and AuNRs by layer-by-layer assembly method. Polyelectrolyte has been used as spacers by some research groups.[41] In this paper, polyelectrolyte multilayers composed of positively charged poly allylamine hydrochloride (PAH) and negatively charged sodium polystyrene sulfonate (PSS) were deposited alternatively on the substrates based on electrostatic interactions. In our experiment, the spacer thickness can be controlled over the nanoscale. The relationship of UV-Vis-NIR absorption properties of AuNRs on silicon substrates and fluorescence emission spectrum of UCNPs is shown in Scheme 1b.

Very recently, we have enhanced 22.6-fold fluorescence in green region by using AuNRs-980 with the aspect ratio of 7.6 with a novel strategy to precisely controlled the spacer thickness by polyelectrolyte multilayers.[33] When the LSPR wavelength of the AuNRs-980 almost overlaps with the excitation of UCNPs, the energy is efficiently collected by AuNRs and transferred from the plasmon nanostructure to the electrons of UCNPs, which leads to an increase of the absorption cross-section of the UCNPs (referred as LFE effect). In this paper, the absorption wavelength of AuNRs-660 with aspect ratio of 3.0 overlaps well with red emission peak of UCNPs (shown in dashed box), which can lead to enhanced red emission due to SPCE effect. Since red emission has deeper tissue penetration capacity than green emission, the design of the heteronanostructures was constructive for bioimaging.

Characterization of AuNRs and UCNPs

We synthesized the AuNRs with three different aspect ratios by seed-mediated growth chemical method, Fig. 1a–c. The shapes

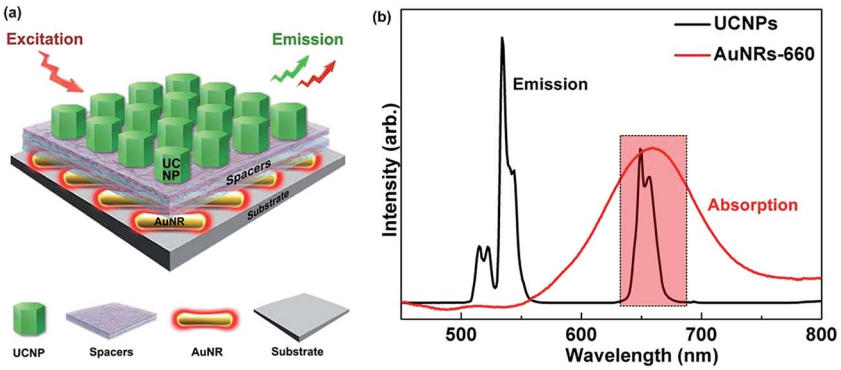

Scheme 1 Experimental strategy and mechanism study of enhanced fluorescence with surface plasmon-coupled emission. (a) Schematic diagram of UCNPs and AuNRs plasmon-enhanced fluorescence system. The UCNPs and AuNRs heteronanostructures were achieved by modulating the thickness of polyelectrolyte multilayers as spacers with layer-by-layer assembly method. (b) UV-Vis-NIR absorption spectrum of AuNRs on silicon substrates and fluorescence emission spectrum of UCNPs. The red emission peak of UCNPs overlaps well with absorption wavelength of AuNRs-660 with aspect ratio 3.0, which can generate surface plasmon-coupled emission effect.

of AuNRs are uniform and the average diameters of the AuNRs are 20.3 ± 1.7, 18.6 ± 2.2 and 14.2 ± 1.8 nm, and the average lengths are 51.6 ± 3.6, 55.2 ± 5.1 and 55.2 ± 8.2 nm (Fig. S1 and Table S1†). The corresponding aspect ratios are 2.6 ± 0.3, 3.0 ± 0.4 and 3.9 ± 0.6, respectively. As shown by UV-Vis-NIR spectrum, the LSPR wavelengths of AuNRs with aspect ratios of 2.6, 3.0 and 3.9 in water are measured to be 670, 725 and 810 nm, respectively (the inset in Fig. 1a–c). The LSPR wavelength of AuNRs exhibits progressive red shift with increasing the aspect ratio. The position of LSPR peak for AuNRs can affect luminescence emission of UCNPs by the electric field coupling effect.

The $NaYF_4$:Yb,Er UCNPs were synthesized using thermal decomposition procedure in a mixed OA/ODE system (Fig. S2†). The HR-TEM image shows the crystal fringes with a distance of 0.515 nm, which is assigned to the (100) crystal plane of the hexagonal phase (Fig. S2c†). The as-synthesized nanocrystals have a hydrophobic surface due to the presence of oleic acid ligands. To obtain hydrophilic UCNPs, we replace oleic acid with polyacrylic acid (PAA) polymer as the new stabilizing ligands (Fig. 1d). The size distribution histograms of UCNPs–PAA are shown in Fig. S3 (ESI†). These nanocrystals are uniform six-prism nanodisks in shape and have an average diameter of 37.5 ± 2.2 nm and height of 29.7 ± 1.7 nm (Table S2†). High-resolution TEM observation of the $NaYF_4$:Yb,Er–PAA reveals that the nanocrystals core with crystal lattice fringe is clearly covered by an amorphous shell due to the presence of PAA coating (the inset of Fig. 1d). The PAA layer on the surface of UCNPs–PAA is very uniform and thin (1.65 ± 0.19 nm). SAED pattern from the $NaYF_4$:Yb,Er layer indicates a polycrystalline feature or many nanoparticles with monocrystalline (Fig. 1e). We also performed Fourier-transform infrared spectroscopy (FT-IR) experiments to confirm PAA coating on the surface of UCNPs (Fig. S4†). The obvious transmission band at 1709 cm^{-1} indicates the existence of –COOH group.[42] Meanwhile, due to PAA modification, the surface charge of UCNPs becomes more negative (from $\zeta = -28.3$ mV to $\zeta = -45.7$ mV), confirming that –COOH group has been successfully grafted onto the nanoparticles (Fig. 1f). This charge alteration allows more effective assembly by electrostatic interactions. In addition, zeta potentials of AuNRs-620, AuNRs-660 and AuNRs-740 are measured to be 41.1, 42.7 and 44.0 mV, respectively (Fig. 1f), indicating their positively charged nature.

Distance-dependent fluorescence enhancement by plasmon nanostructure

Localized surface plasmon excited in noble metal nanoparticles such as Au and Ag results in strong enhancement of electromagnetic field at the surface of these nanostructures.[32] Effective coupling of the enhanced electric field at the surface of the metal nanoparticles with the transition dipole of UCNPs leads to increased absorption cross-section and quantum efficiency of UCNPs.[43] Therefore, noble metal nanoparticles are considered to be a powerful platform to enhance upconversion emission of UCNPs.[32–34]

We fabricated polyelectrolyte multilayer-separated UCNPs and AuNRs heteronanostructures by layer-by-layer assembly method. AuNRs were uniformly coated on the surface of pre-treated silicon substrates as shown by SEM image (Fig. 2a). Compared with corresponding AuNRs in solution (the inset of Fig. 1a–c), the LSPR wavelengths of AuNRs-620, AuNRs-660 and AuNRs-740 deposited on silicon substrates shift toward shorter wavelengths at 620, 660 and 740 nm (Fig. 2b and Table S3†). The shift in the LSPR of AuNRs from solution to silicon substrates results from different local refractive index of the medium around AuNRs.[44] To access the thickness of polyelectrolyte bilayer, the height change at the edge of a scratch was investigated by atomic force microscopy (AFM) (Fig. 2c), which confirms that total thickness of the polyelectrolyte layers is about 10 nm after deposition of ten layer spacers, indicating the thickness of about 1 nm for each monolayer (Fig. 2d).

To investigate the influence of the distance on luminescence behavior, upconversion fluorescence spectra of UCNPs separated from the surface of AuNRs by different thicknesses of polyelectrolyte from 4 to 16 layers are shown in Fig. 2e. Two main peaks at 540 and 650 nm can be identified corresponding

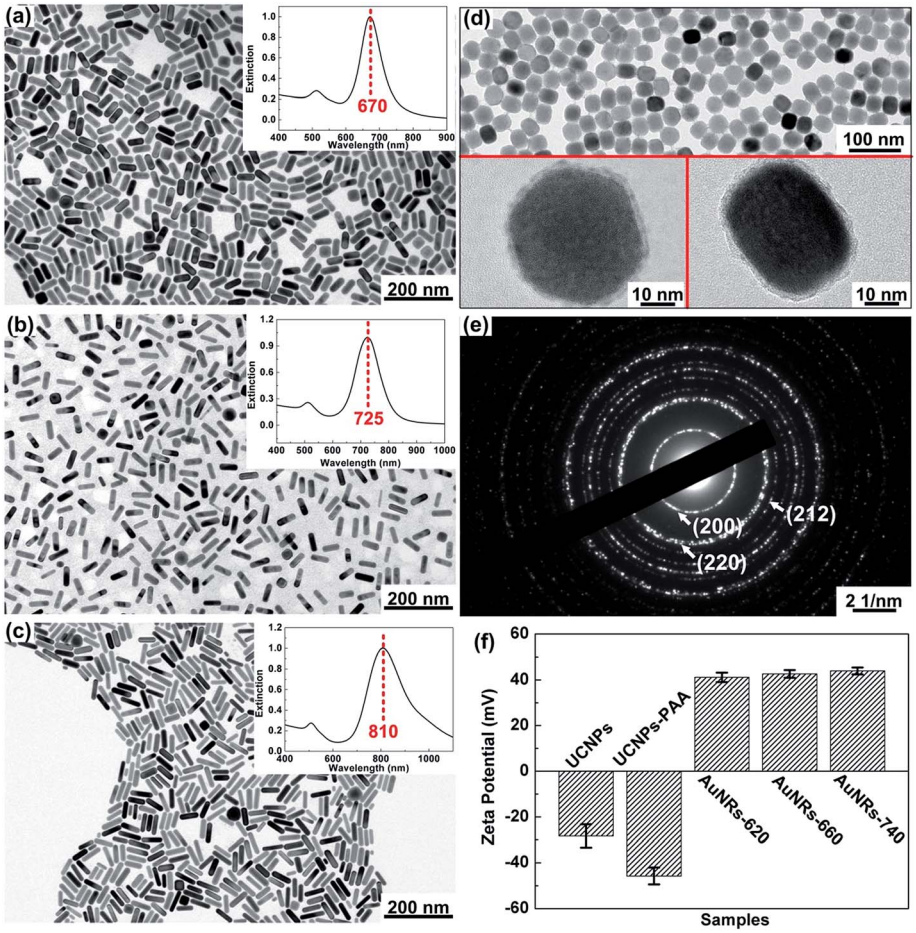

Fig. 1 Characterization of AuNRs and UCNPs nanoparticles. Representative TEM images of: (a) AuNRs-620; (b) AuNRs-660 and (c) AuNRs-740. The inset graphs show UV-Vis-NIR extinction spectra of corresponding AuNRs in solution. (d) TEM image of UCNPs–PAA; The inset graphs were high resolution TEM images of UCNPs–PAA of six-prism underside (left) and of six-prism side (right). (e) Diffraction pattern of UCNPs–PAA; (f) Zeta potentials of UCNPs, UCNPs–PAA and AuNRs with different aspect ratios. It is indicated that UCNPs and UCNPs–PAA are negative-charged and all the AuNRs are positive-charged.

to the (i) $^4S_{3/2} \rightarrow {}^4I_{15/2}$ and (ii) $^4F_{9/2} \rightarrow {}^4I_{15/2}$ transitions, respectively. The existence of polyelectrolytes and AuNRs shows significantly influence on the emission intensity and the ratio of red emission to green emission. And the luminescence enhancement can be optimized by adjusting the distance between $NaYF_4$:Yb,Er nanoparticles and AuNRs through modulating the spacers thickness. It is revealed that the extent of upconversion luminescence enhancement highly depends on the separation distance between the UCNPs and AuNRs in heteronanostructures (Fig. 2e). We obtain fluorescence enhancement factor by dividing integrated fluorescence intensity of the samples with AuNRs enhancement by those without AuNRs enhancement as reference (Ref.). The enhancement factors as the function of the spacer thickness at 540 nm green emission and 650 nm red emission are shown in Fig. 2f. The enhancement factor increases gradually with the spacer thickness increasing from 0 nm to 8 nm, and then decreases subsequently with further increased thickness. The upconversion enhancement factors of UCNPs reach a maximum value of 10.6 for red emission at 650 nm and 5.0 for green emission at 540 nm at the spacer thickness of 8 nm. Saboktakin *et al.*[2] also reported that the luminescence enhancement revealed strongly dependence on the spacer thickness. In case of optimal distance, maximum enhancement factors were 5.2 for Au nanoparticles.[2] Zhang *et al.*[45] also reported that an optimal spacer thickness in $Ag@SiO_2@Y_2O_3$:Er nanoparticles can lead to an emission enhancement factor of 4. Interestingly, we have concluded that the enhancement factors in the red emission region are much larger than those in the green emission region which plays an important role for the deep tissue imaging.

LSPR leads to a number of interesting optical behaviors such as absorption and scattering of excitation light.[46] The fluorescence emission intensity as a result of interaction between metal nanoparticles and fluorescence materials may be achieved from a competition of three effects: (a) local electric field amplification causing increased excitation rate thus increasing fluorescence emission intensity associated with plasmon resonance (LFE effect); (b) surface plasmon-coupled emission effect resulting in increased emission rate contributing to increased luminescence emission intensity (SPCE effect); (c) non-radiative

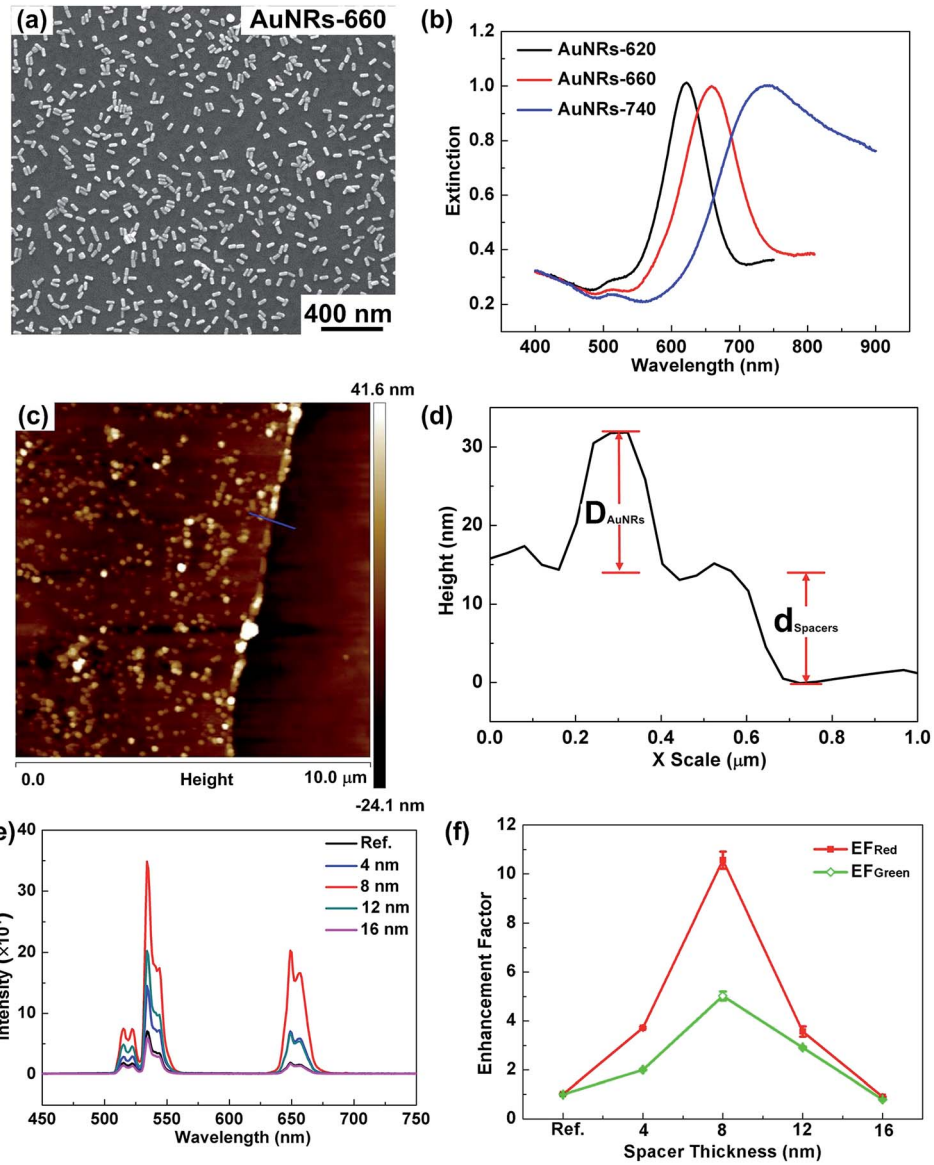

Fig. 2 Distance-dependent surface plasmon-coupled emission enhanced fluorescence analysis. (a) SEM image of AuNRs-660 coated on silicon substrates modified with PSS layer. (b) UV-Vis-NIR extinction spectra of AuNRs with different aspect ratios on silicon substrates. (c) AFM image of a scratch from AuNRs-660 layer on silicon substrates spaced by ten polyelectrolyte layers. (d) Curve of height along the probing path labelled with blue line in (c) (D_{AuNRs} represents the diameter of AuNRs and $d_{Spacers}$ represents the thickness of spacers). (e) Fluorescence spectra of UCNPs separated from the surface of AuNRs by different thicknesses of polyelectrolyte layers. (f) Correlation of the distance between the AuNRs and UCNPs with the enhancement factor collected at 540 nm and 650 nm emission from (e).

energy transfer process from fluorescence materials to metal nanoparticles quenching the luminescence emission (NRET effect).[28,34] In the case of AuNRs-660, the LSPR absorption band (~660 nm) is far away from the excitation wavelength of UCNPs (~980 nm). Therefore, the enhanced excitation efficiency due to LFE effect is expected to play a negligible role for luminescence enhancement. When AuNRs-660 is placed nearby UCNPs, SPCE effect can be a remarkable mechanism to enhance upconversion luminescence since the red emission band of UCNPs overlaps well with the LSPR wavelength of AuNRs-660.[14,24,32,47,48] This enhancement is also attributed to the strong gold plasmon resonance scattering and high ratio of scattering/absorption.[45,49]

It has also been demonstrated that core–shell nanoparticles modified with Au or Ag result in enhanced upconversion fluorescence emission intensity.[50] Therefore, some papers have investigated the effect of core–shell nanostructures on fluorescent intensity by silicon coating between UCNPs and Au nanoparticles. For example, Xu *et al.*[34] have prepared $NaYF_4$:Yb,Er@SiO_2@Ag core–shell nanocomposites. They observed a maximum fluorescence enhancement of 14.4-fold in the case of 15 nm thickness Ag coating and 10.8-fold in the case of 30 nm thickness Ag coating. In a different structure, Zhang *et al.*[45] prepared Ag@SiO_2@Y_2O_3:Er core–shell–shell nanoparticles with a maximum fluorescence enhancement factor of

4. Ge *et al.*[28] also demonstrated that the fluorescence emission of $Au@SiO_2@Y_2O_3$:Yb/Er can be enhanced by 9.5-fold. These results proved that Au or Ag nanoparticles could enhance the UCL intensity.

Spectra-dependent fluorescence enhancement by AuNRs with different aspect ratios

We investigated spectra-dependent luminescence enhancement with the thickness of polyelectrolyte multilayers of 8 nm. Fluorescence spectroscopic analysis is shown in Fig. 3a. The enhancement factors are 4.9, 10.6 and 1.7 for UCNPs plasmon-coupled with AuNRs-620, AuNRs-660 and AuNRs-740 at 650 nm red emission peak, respectively (Fig. 3b). It should be noticed that for the AuNRs with different aspect ratios, the enhancement factors for red emission are larger than that of green emission. Compared with the reference (indicated as Ref. in the figure), UCNPs with AuNRs-660 and AuNRs-620 plasmon nanoparticles have achieved obvious upconversion emission enhancement effect. As expected, there has little emission enhancement in the case of AuNRs-740 plasmon nanostructures.

AuNRs possess special LSPR wavelength at 600–1200 nm which are in dependent of their aspect ratios.[29] Luminescence enhancement depends strongly on the scattering efficiency with optimized aspect ratio of 3.4 for AuNRs.[27,51] AuNRs with diameters in the range of 10–20 nm also contribute to the relatively strong luminescence enhancement.[52] Hence, AuNRs with diameters of 10–20 nm and aspect ratio of 2–4 used in this paper can facilitate strong emission enhancement. Metal nanostructures can affect the luminescence of UCNPs in two different effects including increased the excitation rate of UCNPs by the electric fields (LFE effect) and the increased emission rate by quantum yield of UCNPs (SPCE effect).[22] Excitation and emission enhancement effects arise from the spectral overlap of LSPR wavelength of metal nanoparticles with the excitation or the emission of UCNPs, respectively. Since LSPR wavelengths of all the AuNRs nanostructures cannot overlap with the excitation laser of UCNPs (about 980 nm), the luminescence enhancement is attributed mainly to emission enhancement effects. Spectroscopic analysis shows that the fluorescence enhancement has significantly spectral dependence, suggesting that SPCE effect plays an important role in the emission enhancement. In fact, LSPR wavelength of special AuNRs-660 matches with red emission peaks of UCNPs in 650 nm, the maximum quantum efficiency and emission enhancement are produced. For UCNPs with AuNRs-740 enhancement, the LSPR wavelength of this AuNRs has little overlap with emission peak of UCNPs, resulting in limited fluorescence enhancement. Meanwhile, AuNRs-620 generates ~4.9-fold fluorescence enhancement since LSPR wavelength partially overlaps with the emission of UCNPs.

Fluorescence lifetime

To investigate the upconversion process of UCNPs and the mechanism of AuNRs plasmon enhancement, we have observed fluorescence lifetime of UCNPs with and without AuNRs nanostructures using a time-resolved fluorescence spectrometer equipped with a 980 nm pulse laser. Fig. 4a shows the luminescence decay curves collected from the UCNPs with and without AuNRs-660 spaced by 8 nm polyelectrolyte multilayers at red emission at 650 nm. Unlike the downconversion luminescence materials whose decay curves can be fitted as an exponential function, the decay curve of UCNPs is relatively complicated and cannot be fitted as mono-exponential function.[25,53] These phenomena may due to the fact that the upconversion luminescence is not only decided by the first excited level of Er^{3+} and Yb^{3+} ions and their energy transfer process, but also related to the lifetime of the second excited level of Er^{3+} ions.[25,53] Therefore, we have achieved the decay time of UCNPs using the half of its maximal value according to the ref. 25 and 53 Fig. 4b and c shows the fluorescence lifetime as the function of spacer thickness and different AuNRs. With the increase of spacer thickness, the decay time of the red emission decreases, reaching minimum values at a thickness of 8 nm, and then increases when the spacer thickness further increased to 16 nm (Fig. 4b). Especially, we obtain that the decay time is 374.0 μs for UCNPs without AuNRs enhancement, while the decay time decreases to the minimal value of 299.1 μs in the case of AuNRs-660 enhancement (Fig. 4b). For UCNPs with the AuNRs enhancement, the decrease of decay time and thus increase of radiative decay rate are consistent with the electromagnetic field coupling of fluorescence emission with surface

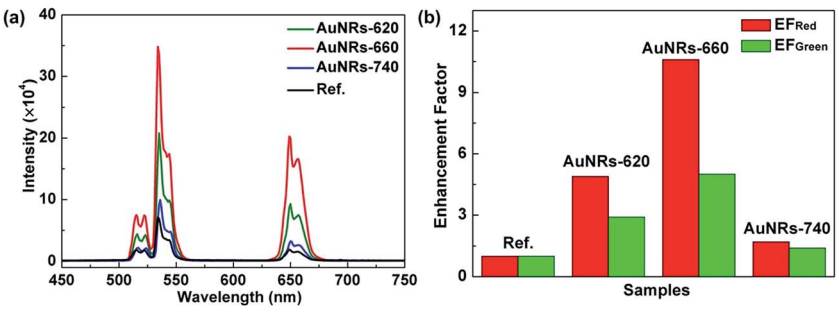

Fig. 3 Spectra-dependent enhanced fluorescence with surface plasmon-coupled emission. (a) Fluorescence spectra of UCNPs deposited on AuNRs-620, AuNRs-660 and AuNRs-740 spaced by 8 polyelectrolyte layers. (b) Histogram of the AuNRs with enhancement factors for red emission of 650 nm and green emission of 540 nm.

plasmon resonance of AuNRs and a metal-induced Purcell effect.[2] In fact, both the radiative and non-radiative decay rates of the UCNPs can be tuned in the presence of AuNRs-660. In very close proximity, the non-radiative decay process arisen from the energy transfer from UCNPs to AuNRs dominates and causes finally very less fluorescence enhancement effect.[8] With the increasing distance, radiative decay and non-radiative decay rate can become slow. However, non-radiative decay rate decreases more quickly compared to the radiative decay rates. Therefore, the radiative decay rate becomes a key factor contributing to the enhanced fluorescence. At very large distances (~16 nm), AuNRs-660 produces negligible effect on both the radiative decay rate and non-radiative decay rate, and then the upconversion luminescence drops almost to the reference level.

Since the LSPR wavelength of AuNRs-660 overlaps well with the red emission at 650 nm, UCNPs enhanced with AuNRs-660 have the shortest decay time, thus producing the strongest emission enhancement (Fig. 4c). In the case of AuNRs-620 nanoparticles, LSPR wavelength has a partial overlap with red emission, resulting in partial decrease in decay time as compared with the reference samples (Fig. 4c). For UCNPs and AuNRs-740 plasmon nanostructures, the LSPR wavelength of AuNRs-740 is away from the red emission of UCNPs and no significant decrease of the decay time is achieved. The decrease of decay time may be attributed to SPCE effect.[28,54] The decrease in decay time is also due to the alteration of the permittivity of surrounding the emitters resulting in an increase of quantum yield.[26] In addition, AuNRs can introduce an additional non-radiative decay channel which facilitates the decrease in the decay time of UCNPs.[54] In fact, when UCNPs are located in the proximity of the plasmon nanostructures, it becomes more possible that a second energy transfer step which further excites the Er^{3+} ion by the transition $^4I_{11/2} \rightarrow {}^4F_{7/2}$ before the non-radiative decay $^4I_{11/2} \rightarrow {}^4I_{13/2}$ and is accompanied by emitting the red light at $^4F_{9/2}$ level.[54]

Theoretical simulation explaining luminescence enhancement mechanism

When $NaYF_4$:Yb,Er UCNPs are located in the vicinity of metal nanoparticles, light collection is enhanced by sensitizer due to the effective coupling effect between the electric field of UCNPs and metal nanoparticles, thereby leading to luminescence enhancement.[32,55] To deeply understand the complex interaction, the square of electric field, quantum efficiency and emission enhancement as a function of the distance between UCNPs and AuNRs were theoretically simulated (Fig. 5). To simplify the experimental condition, we placed the UCNPs as emission dipoles in the most remarkable enhancement position relative to AuNRs and then simulated the fluorescence enhancement effect. The fluorescence emission intensity (I) of UCNPs can be estimated by the following eqn (1):[32]

$$I = \phi\sigma_S\eta_{ET}\varphi_A \quad (1)$$

where ϕ is the photon flux of the excitation light, σ_S is the absorption cross-section of the lanthanide-doped ion as sensitizer, η_{ET} is the total energy transfer efficiency from sensitizer to activator, and φ_A is the quantum yield of activator. The local electric field (E) induced by LSPR effect from AuNRs can enhance the photon flux (ϕ) of excitation laser, which is proportional to $|E|^2$ by eqn (2):[32]

$$\phi \propto |E|^2 \quad (2)$$

In this paper, simulated electric field distribution surrounding AuNRs was obtained by Finite Element Method (FEM) (Fig. 5a–c). We plotted the relationship of the square of electric field surrounding the AuNRs *versus* the distance according to electromagnetic methods (Fig. 5d). As the distance increases, the square of electric field decreases, reaching a minimum value nearly zero. In the case of the samples with AuNRs-740, AuNRs-660 and AuNRs-620 enhancement, the square of the electric field intensity reduces rapidly when the distance is set less than 5 nm. Therefore, with the increase of distance, the photon flux decreases rapidly since it is proportion to $|E|^2$.

The existence of coupling occurring between the phonons and electrons can also enhance the radiative decay rate of activator ions in UCNPs, which modifies the photon-mode density of luminescence nanomaterials.[32] Thus the quantum yield (φ_A) can be obtained as:[32]

$$\varphi_A = \frac{k_r + k_m}{k_r + k_m + k_{nr}} \quad (3)$$

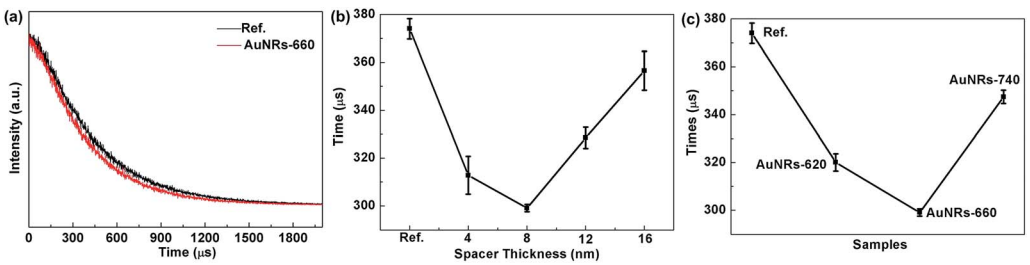

Fig. 4 Fluorescence lifetime analysis. (a) Fluorescence decay curves at 650 nm ($^4F_{9/2}$ to $^4I_{15/2}$ transition) for UCNPs with and without AuNRs-660 enhancement. (b) Decay time as a function of the thickness of polyelectrolyte multilayers, which was enhanced by AuNRs-660. (c) Decay time as a function of different aspect ratios of AuNRs, which was spaced by 8 nm thickness of polyelectrolyte multilayers. All the data were measured under the 980 nm laser excitation.

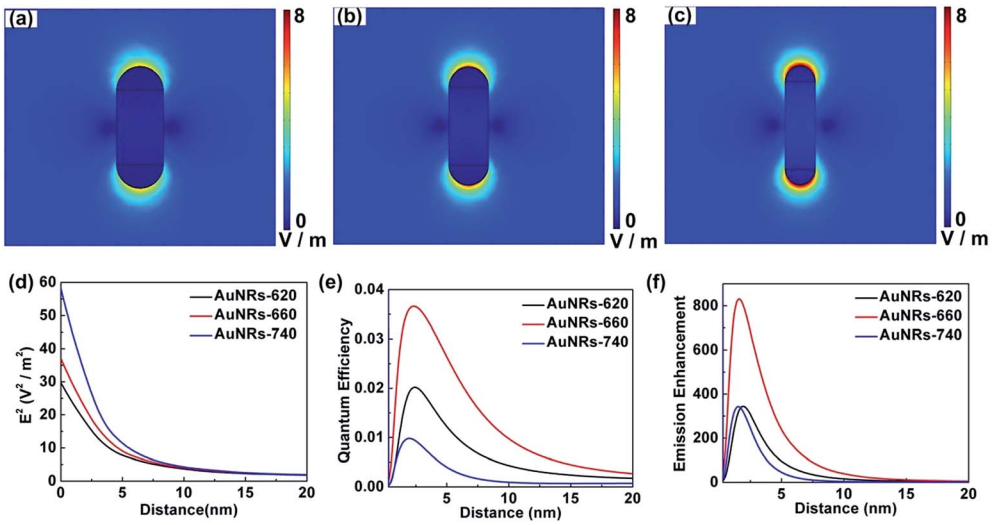

Fig. 5 Theoretical simulation explaining enhancement mechanism. Simulated electric field distribution surrounding: (a) AuNRs-620; (b) AuNRs-660 and (c) AuNRs-740. (d) Square of electric field; (e) quantum efficiency and (f) emission enhancement as a function of distance between of AuNRs and UCNPs, respectively.

where k_r, k_{nr}, and k_m are the radiative decay rate, non-radiative decay rate and metal-induced additional radiative decay rate, respectively.[32] If the UCNPs and metal nanoparticles are placed within very close distance, direct electron transfer can lead to quenching of the upconversion luminescence.[32] To obtain enhanced quantum efficiency, optimal distance between UCNPs and AuNRs is a key factor for the purpose of decreasing non-radiative and increasing radiative decay rates.[32,56] Fig. 5e shows the quantum efficiency of a dipole emitter as a function of the distance enhanced by AuNRs with three different aspect ratios. It is indicated that the largest quantum efficiency can be obtained when the distance is modulated to 2.3 nm with AuNRs-660 enhancement. UCNPs have the quantum efficiency of about 1% in the absence of AuNRs, while quantum efficiency of UCNPs reaches 3.7% in the presence of AuNRs-660. The quantum efficiency enhancement can be explained by the dipole model presented by Gersten and Nitzan.[57]

According to eqn (1), the emission enhancement is obtained by the product of the square of electric field and quantum efficiency, which is highest when UCNPs are placed in proximity to AuNRs-660 (Fig. 5f). An optimal distance of 1.58 nm for emission enhancement can be identified in the case of AuNRs-660. It can be concluded that the distance-dependence of the maximum emission enhancement is attributed to the synchronous effect of the non-resonant absorption enhancement at 980 nm and resonant emission enhancement at 650 nm. Marjan *et al.*[2] also pointed out that the upconversion emission enhancement by Au nanoparticles can be explained by two different process including enhanced electric field and quantum efficiency. In addition, since the absorption process of UCNPs is a sequential and non-coherent process and LSPR wavelengths of all the AuNRs have no resonance with the excitation frequency, plasmon enhancement to increase energy transfer between atoms in UCNPs appears impossible.

There are many factors which can influence the theoretical simulation results, such as the relative positions of UCNPs and AuNRs, electric field coupling of near placed AuNRs, the surface effect of nanoparticles, the reflectance of silicon substrates and the refraction of polymer dielectric layers.[58] The results of simulated optimal distance inconsistent with experimental data may be attributed to the predigestion of the models. However, the model provides mechanistic insight into the facts that both electric field distribution and quantum efficiency are the main factors that determine the enhancement factors by AuNRs with different aspect ratios. The model also indicates that efficiency in enhancement can be maximized when the LSPR wavelength matches well with the emission wavelength.

Tissue penetration capacity measurement

To further demonstrate the capability of polyelectrolyte multilayer-separated UCNPs and AuNRs heteronanostructures in deep tissue imaging, we measured penetration depth at red emission of 650 nm using homogeneous nylon panels with different thickness (5–12.5 mm), Fig. 6. Nylon phantom is a proper tissue phantom to analyze penetration depth due to its similar scattering properties and optical behaviors with native tissues.[59] As shown by luminescence graphs by post-treatment using pseudo-color form, we observed much deeper tissue penetration for the UCNPs with AuNRs enhancement at spacer thickness of 8 nm (Fig. 6a–d) than those without AuNRs enhancement (Fig. 6e–h). We quantitatively studied the radiance as the function of penetration depth at 650 nm red emission. It is indicated that the radiances for the substrates of SPCE and Ref. decrease when the penetration depth is increased gradually (Fig. S5†). The tissue penetration depth for UCNPs enhanced by AuNRs-660 achieves a maximal value of 12.5 mm, and this depth for UCNPs with no AuNRs plasmon nanostructures is only 7.5 mm. These results theoretically verify that

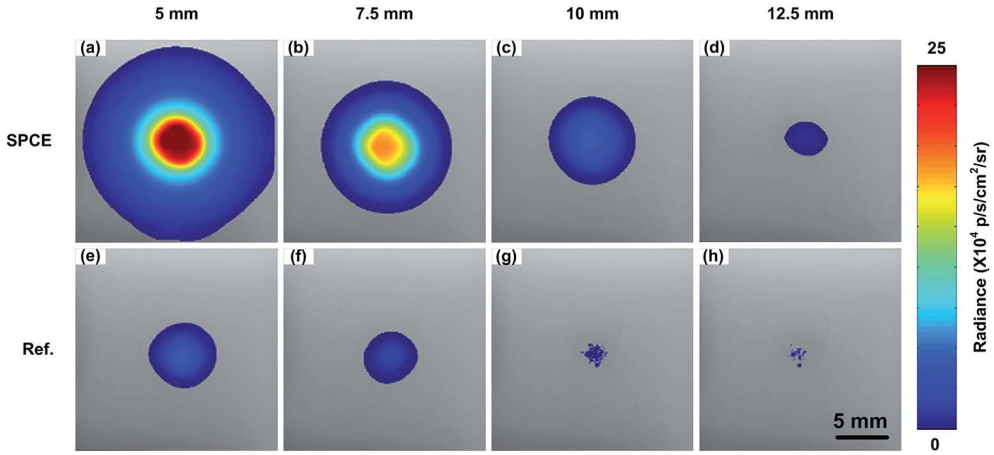

Fig. 6 Tissue penetration capacity for the bioimaging applications. The samples were (a–d) the UCNPs in combination with plasmon nanostructures of AuNRs-660 spaced by 8 nm polyelectrolyte multilayers and (e–h) only UCNPs as reference (Ref.) collected at red emission at 650 nm. The penetration depth was (a and e) 5 mm, (b and f) 7.5 mm, (c and g) 10 mm and (d and h) 12.5 mm.

UCNPs could have a deeper tissue penetration capacity when enhanced by SPCE effect of AuNRs.

Conclusions

Lanthanide-doped upconversion nanoparticles can convert NIR light excitation into visible emission by upconversion process, but their quantum yield is relatively low. So fluorescence emission especially red emission of the novel nanoprobes of UCNPs need to be enhanced. Putting UCNPs surrounding metal nanoparticles will largely concentrate electric fields at nanoscale-volume, thus leading to fluorescence enhancement of UCNPs. To improve the quantum yield and enhance the red emission, we demonstrated an effective strategy to fabricate polyelectrolyte separated UCNPs and AuNRs heteronanostructures using layer-by-layer assembly method. Polyelectrolyte multilayers are used to tune precisely interparticles distance at nanometer scale. Specifically, we used AuNRs with aspect ratio of 3.0 to enhance red emission of UCNPs for deep-tissue bioimaging. The luminescence enhancement factors of UCNPs are dependent mainly upon the spacers thickness and the optical properties of metal nanoparticles of AuNRs. A maximum luminescence enhancement could be achieved when the distance was modulated as 8 nm. The maximum overlap of the LSPR wavelength of AuNRs with red emission of UCNPs results in maximum upconversion enhancement up to 10.6-fold for the red emission at 650 nm. The mechanism is explained by the increased radiative decay rate of Er^{3+} doped in the UCNPs. Computational electromagnetic simulations further confirm that AuNRs can enhance the quantum efficiency and thus the fluorescence emission of UCNPs. We also demonstrate the heteronanostructures enable deep-tissue imaging. Therefore, our findings may provide a unique platform for rationally enhancing the upconversion emission and can widely impact on various areas of bioimaging, solar energy and other engineering applications.

Acknowledgements

This work was financially supported by the National Natural Science Foundation of China (11372243, 81001669, 11532009, 11522219), International Science & Technology Cooperation Program of China (2013DFG02930), National Key Scientific Apparatus Development of Special Item (2013YQ190467), Natural Science Basic Research Plan in Shaanxi Province of China (2014JQ6199, 2015JM5215), the Fundamental Research Funds for the Central Universities (2012jdhz46). M.L. is supported by scholarship from the China Scholarship of Council. The SEM and TEM work was done at International Center for Dielectric Research (ICDR), Xi'an Jiaotong University, Xi'an, China. The authors also thank Ms Dai Yan Zhu, Ms Lu Lu and Mr Ma Chuan Sheng for their help in using SEM and TEM.

Notes and references

1 K. König, *J. Microsc.*, 2000, **200**, 83–104.
2 M. Saboktakin, X. Ye, S. J. Oh, S. H. Hong, A. T. Fafarman, U. K. Chettiar, N. Engheta, C. B. Murray and C. R. Kagan, *ACS Nano*, 2012, **6**, 8758–8766.
3 F. Wang, D. Banerjee, Y. Liu, X. Chen and X. Liu, *Analyst*, 2010, **135**, 1839–1854.
4 H. S. Mader, P. Kele, S. M. Saleh and O. S. Wolfbeis, *Curr. Opin. Chem. Biol.*, 2010, **14**, 582–596.
5 F. Wang and X. G. Liu, *Chem. Soc. Rev.*, 2009, **38**, 976–989.
6 J. Shen, L. Zhao and G. Han, *Adv. Drug Delivery Rev.*, 2013, **65**, 744–755.
7 J. C. Boyer and F. C. J. M. v. Veggel, *Nanoscale*, 2010, **2**, 1417.
8 J. Shen, Z. Li, Y. Chen, X. Chen, Y. Chen, Z. Sun and S. Huang, *Appl. Surf. Sci.*, 2013, **270**, 712–717.
9 C. Liu, L. Zhang, Q. Zheng, F. Luo, Y. Xu and W. Weng, *Sci. Adv. Mater.*, 2012, **4**, 1–22.
10 F. Wang, R. Deng, J. Wang, Q. Wang, Y. Han, H. Zhu, X. Chen and X. Liu, *Nat. Mater.*, 2011, **10**, 968–973.

11 H. Schäfer, P. Ptacek, O. Zerzouf and M. Haase, *Adv. Funct. Mater.*, 2008, **18**, 2913–2918.
12 S. Schietinger, L. D. S. Menezes, B. R. Lauritzen and O. Benson, *Nano Lett.*, 2009, **9**, 2477–2481.
13 F. Wang, R. Deng, J. Wang, Q. Wang, Y. Han, H. Zhu, X. Chen and X. Liu, *Nat. Mater.*, 2011, **10**, 968–973.
14 J. Zhou, Z. Liu and F. Y. Li, *Chem. Soc. Rev.*, 2012, **41**, 1323–1349.
15 G. Chen, T. Y. Ohulchanskyy, R. Kumar, H. Ågren and P. N. Prasad, *ACS Nano*, 2010, **4**, 3163–3168.
16 Y. Bai, Y. Wang, K. Yang, X. Zhang, G. Peng, Y. Song, Z. Pan and C. H. Wang, *J. Phys. Chem. C*, 2008, **112**, 12259–12263.
17 D. Chen, Y. Yu, F. Huang and Y. Wang, *Chem. Commun.*, 2011, **47**, 2601–2603.
18 F. Wang, J. Wang and X. Liu, *Angew. Chem., Int. Ed.*, 2010, **49**, 7456–7460.
19 G. Chen, H. Qiu, P. N. Prasad and X. Chen, *Chem. Rev.*, 2014, **114**, 5161–5214.
20 G. S. Yi and G. M. Chow, *Chem. Mater.*, 2007, **19**, 341–343.
21 H. X. Mai, Y. W. Zhang, L. D. Sun and C. H. Yan, *J. Phys. Chem. C*, 2007, **111**, 13721–13729.
22 N. J. Greybush, M. Saboktakin, X. Ye, C. Della Giovampaola, S. J. Oh, N. E. Berry, N. Engheta, C. B. Murray and C. R. Kagan, *ACS Nano*, 2014, **8**, 9482–9491.
23 L. Sudheendra, V. Ortalan, S. Dey, N. D. Browning and I. M. Kennedy, *Chem. Mater.*, 2011, **23**, 2987–2993.
24 H. Zhang, Y. J. Li, I. A. Ivanov, Y. Q. Qu, Y. Huang and X. F. Duan, *Angew. Chem., Int. Ed.*, 2010, **49**, 2865–2868.
25 W. Zhang, F. Ding and S. Y. Chou, *Adv. Mater.*, 2012, **24**, OP236–OP241.
26 M. Saboktakin, X. Ye, U. K. Chettiar, N. Engheta, C. B. Murray and C. R. Kagan, *ACS Nano*, 2013, **7**, 7186–7192.
27 C. Zhang and J. Y. Lee, *J. Phys. Chem. C*, 2013, **117**, 15253–15259.
28 W. Ge, X. Zhang, M. Liu, Z. Lei, R. Knize and Y. Lu, *Theranostics*, 2013, **3**, 282.
29 P. Kannan, F. Abdul Rahim, R. Chen, X. Teng, L. Huang, H. Sun and D. H. Kim, *ACS Appl. Mater. Interfaces*, 2013, **5**, 3508–3513.
30 H. Y. Xing, W. B. Bu, S. J. Zhang, X. P. Zheng, M. Li, F. Chen, Q. J. He, L. P. Zhou, W. J. Peng, Y. Q. Hua and J. L. Shi, *Biomaterials*, 2012, **33**, 1079–1089.
31 P. Anger, P. Bharadwaj and L. Novotny, *Phys. Rev. Lett.*, 2006, **96**, 113002.
32 S. Han, R. Deng, X. Xie and X. Liu, *Angew. Chem., Int. Ed.*, 2014, **53**, 11702–11715.
33 A. L. Feng, M. L. You, L. Tian, S. Singamaneni, M. Liu, Z. Duan, T. J. Lu, F. Xu and M. Lin, *Sci. Rep.*, 2015, **5**, 7779.
34 P. Yuan, Y. H. Lee, M. K. Gnanasammandhan, Z. Guan, Y. Zhang and Q. H. Xu, *Nanoscale*, 2012, **4**, 5132–5137.
35 Z. Li, L. Wang, Z. Wang, X. Liu and Y. Xiong, *J. Phys. Chem. C*, 2011, **115**, 3291–3296.
36 W. Fan, B. Shen, W. Bu, F. Chen, K. Zhao, S. Zhang, L. Zhou, W. Peng, Q. Xiao and H. Xing, *J. Am. Chem. Soc.*, 2013, **135**, 6494–6503.
37 N. R. Jana, L. Gearheart and C. J. Murphy, *J. Phys. Chem. B*, 2001, **105**, 4065–4067.
38 B. Nikoobakht and M. A. El-Sayed, *Chem. Mater.*, 2003, **15**, 1957–1962.
39 P. G. Etchegoin, E. C. Le Ru and M. Meyer, *J. Chem. Phys.*, 2006, **125**, 164705.
40 H. Mertens, A. F. Koenderink and A. Polman, *Phys. Rev. B: Condens. Matter Mater. Phys.*, 2007, **76**, 115123.
41 G. M. Lowman, S. L. Nelson, S. M. Graves, G. F. Strouse and S. K. Buratto, *Langmuir*, 2004, **20**, 2057–2059.
42 S. Wu, N. Duan, X. Ma, Y. Xia, H. Wang and Z. Wang, *Anal. Chim. Acta*, 2013, **782**, 59–66.
43 A. Priyam, N. M. Idris and Y. Zhang, *J. Mater. Chem.*, 2012, **22**, 960–965.
44 C. D. Chen, S. F. Cheng, L. K. Chau and C. R. C. Wang, *Biosens. Bioelectron.*, 2007, **22**, 926–932.
45 F. Zhang, G. B. Braun, Y. Shi, Y. Zhang, X. Sun, N. O. Reich, D. Zhao and G. Stucky, *J. Am. Chem. Soc.*, 2010, **132**, 2850–2851.
46 A. Tao, P. Sinsermsuksakul and P. Yang, *Nat. Nanotechnol.*, 2007, **2**, 435–440.
47 J. Lakowicz, *Plasmonics*, 2006, **1**, 5–33.
48 N. Liu, W. P. Qin, G. S. Qin, T. Jiang and D. Zhao, *Chem. Commun.*, 2011, **47**, 7671–7673.
49 G. Schneider, G. Decher, N. Nerambourg, R. Praho, M. H. V. Werts and M. Blanchard-Desce, *Nano Lett.*, 2006, **6**, 530–536.
50 S. Han, R. Deng, X. Xie and X. Liu, *Angew. Chem., Int. Ed.*, 2014, **53**, 11702–11715.
51 K. S. Lee and M. A. El-Sayed, *J. Phys. Chem. B*, 2006, **110**, 19220–19225.
52 M. Hu, C. Novo, A. Funston, H. Wang, H. Staleva, S. Zou, P. Mulvaney, Y. Xia and G. V. Hartland, *J. Mater. Chem.*, 2008, **18**, 1949–1960.
53 Z. Q. Li, S. Chen, J. J. Li, Q. Q. Liu, Z. Sun, Z. B. Wang and S. M. Huang, *J. Appl. Phys.*, 2012, **111**, 014310.
54 S. Schietinger, T. Aichele, H. Q. Wang, T. Nann and O. Benson, *Nano Lett.*, 2010, **10**, 134–138.
55 W. Deng, F. Xie, H. T. Baltar and E. M. Goldys, *Phys. Chem. Chem. Phys.*, 2013, **15**, 15695–15708.
56 K. Aslan, I. Gryczynski, J. Malicka, E. Matveeva, J. R. Lakowicz and C. D. Geddes, *Curr. Opin. Biotechnol.*, 2005, **16**, 55–62.
57 J. Gersten and A. Nitzan, *J. Chem. Phys.*, 1981, **75**, 1139–1152.
58 S. Bhowmick, S. Saini, V. B. Shenoy and B. Bagchi, *J. Chem. Phys.*, 2006, **125**, 181102.
59 X. Ma, F. Kang, F. Xu, A. Feng, Y. Zhao, T. Lu, W. Yang, Z. Wang, M. Lin and J. Wang, *PLoS One*, 2013, **8**, e77926.